HOKKAIDO UNIVERSITY

Title	A kinetic model of the dissolution of copper(II) oxide in EDTA solutions considering the coupling of metal and oxide ion transfer
Author(s)	Tamura, Hiroki; Ito, Naotsugu; Kitano, Masahiko; Takasaki, Shinichi
Citation	Corrosion Science, 43(9), 1675-1691 https://doi.org/10.1016/S0010-938X(00)00171-2
Issue Date	2001-09
Doc URL	http://hdl.handle.net/2115/52958
Type	article (author version)
File Information	CuO dissln model.pdf

Instructions for use

Hokkaido University Collection of Scholarly and Academic Papers : HUSCAP

A kinetic model of the dissolution of copper(II) oxide in EDTA solutions considering the coupling of metal and oxide ion transfer

Hiroki Tamura [a,*], Naotsugu Ito [a], Masahiko Kitano [a], Shinichi Takasaki [b]

[a] *Research Group of Materials Chemistry, Graduate School of Engineering, Hokkaido University, Saporo, Hokkaido 060-8628, Japan*

[b] *Kurita Central Laboratories, Kurita Water Industries Ltd., 7-1, Wakamiya, Morinosato, Atsugi, Kanagawa 243-0124, Japan*

*Corresponding author. Tel.: +81-11-613-1361; fax: +81-11-613-1361

E-mail address: h-tamura@eng.hokudai.ac.jp (H. Tamura)

Abstract

The dissolution of metal oxides in solutions is related to the durability of protective oxide films on metals and the removal of corrosion scales on steels, and is important in corrosion science and corrosion protection engineering. In the study here, copper(II) oxide was sintered in a disk shape to maintain a constant surface area throughout dissolution, and concentration of Cu(II) dissolved in EDTA solutions was measured as a function of time for different pH and EDTA concentrations at 80°C. Generally, only initial dissolution rates have been the object of study, but here the dissolution rate throughout the run could be examined. Without EDTA CuO did not dissolve, but with EDTA the dissolved Cu(II) concentration increased with time linearly at pH ≤ 7 and in a parabolic manner at pH ≥ 8.5. The dissolution rate increased with increasing pH at pH ≤ 7, but it decreased with pH at pH ≥ 8. As a result the concentration of dissolved Cu(II) at a specific time showed a peak at pH 7-8. Assessment and prediction of the extent of dissolution for given times, pH, EDTA concentrations, etc. with a model would be valuable for engineering purposes. A kinetic model is proposed by assuming the following successive elementary steps: (1) the transfer of Cu(II) ions as EDTA chelates CuY^{2-} to the solution leaving reactive and unstable "lone oxide ions" $–O^{2-}$ on CuO with a backward reaction, and this is coupled with (2) the reaction of the "lone oxide ions" with protons to form water. The derived rate equation reproduced the linear and parabolic time changes in the dissolved Cu(II) concentration and the dissolution peak at pH 7-8. The deviation from linearity in the alkaline range is due to the increasing backward reaction in step (1). From the pH dependence of the model parameters, the H_2Y^{2-} and HY^{3-} were estimated to be the dissolving EDTA species in solution.

Keywords: Copper(II) oxide; EDTA; Chelate; Dissolution; Kinetics; Modeling

1. Introduction

Corrosion of metals can be prevented by protective oxide films (passivating films). The formation and stability of such films are affected by the dissolution of oxides in aqueous solutions, and the dissolution of oxides is important in corrosion science and corrosion protection engineering. Also, the dissolution of metal oxides has been applied to the removal of steel millscale and recently to the removal of radioactive contamination in nuclear power plants. The radioactive contamination is caused by the incorporation of radioactive isotope ions into oxide scales formed on pipes and turbine blades by corrosion. Contaminated oxide scales are dissolved and washed away with solutions containing chelating agents like EDTA, citric acid, oxalic acid, and others.
In these solutions oxides dissolve due to complexation in weakly acidic environments where the solubility of the oxides is very low without the chelating agents. It is considered that the dissolution of substrate metals which would occur with strong acids can be minimized with weak acids such as chelating agents.

Leaching of ores in hydrometallurgy, removal of metal ion contaminants in semiconductor wafers, evaluation of water quality which is affected by the weathering of rocks, and sample preparation for wet analysis are other examples of the application of metal oxide dissolution.

In the metal oxide dissolution applications described above, a theory or model would enable a quantitative evaluation of the extent of dissolution under given conditions. Industrial processes involving metal oxide dissolution could be designed and controlled by the results of theoretical evaluations. Assessment and prediction of the quality of environmental waters will also benefit from a quantitative evaluation of the dissolution of oxides.

To model the dissolution of metal oxides the kinetics of dissolution must be established, and there are many reviews and books describing the kinetics of oxide dissolution [1-15]. The rate of dissolution is affected by various factors, and there are several types of dissolved metal ion concentration vs. time curves [14]: deceleratory (typically the parabolic rate law); sigmoidal (typically the Avrami-Erofejev law); geometric (the cube-root rate law for the complete dissolution and zero-order rate law for dissolution small enough to cause little change in the surface area); and acceleratory. It is considered that the type of rate law obeyed by an oxide can change depending on

the distribution of particle sizes and shapes and also depending on the particle bulk anisotropy in crystal structures, chemical composition, etc. To model the kinetics of dissolution of powder oxide samples where individual oxide particles behave independently, the effect of external and internal heterogeneity of particles on the dissolution rate must be considered.

The dissolution rate is also affected by solution conditions, and the solution pH is an important variable of aqueous solutions. One unique feature of the effect of pH on the rate of dissolution by chelating agents with and without reducing agents and light irradiation is that the dissolution rate reaches a maximum at a specific pH. The systems for which a pH peak has been observed include: Fe(III) (hydr)oxides cysteine [16]; goethite (α-FeOOH) by phenolic compounds [17] and oxalic acid [18]; akaganeite (β-FeOOH) by EDTA [19]; hematite (α-Fe_2O_3) by EDTA [20] and oxalic and citric acids [21]; magnetite (Fe_3O_4) by EDTA [22-26], thioglycolic acid [27], oxalic acid [28], NTA [29], mercaptocarboxylic acids [30], and thioglycolic acid with anionic polyelectrolytes [31]; and cobalt ferries ($Co_xFe_{3-x}O_4$) by thioglycolic acid [32].

The pH peak has been explained by the effect of pH on the speciation of both chelating agents in solution and also surface hydroxyl sites on oxides, which affect the formation of surface complexes between ligands and surface sites as intermediates preliminary to dissolution [14,27,30,31]. The adsorption of chelating agents on oxides has been studied [33-37], and characterization of ligand-surface complexes by ex situ spectroscopic methods has also been made [38]. The pH dependence of dissolution and adsorption has been reported to be parallel [21], but elsewhere apparently it was not [39,40].

To correlate dissolution ad adsorption for explaining the pH peak, most papers consider the effect of the surface potential, changes in elementary reactions of different surface species, the synergetic role of protons or hydroxide ions in the surface complexation, and/or a special relationship between the dissolution peak pH and the deprotonation constants of ligands and surface hydorxyl sites. As a result the reaction mechanisms are very complex. Further, these mechanisms are mostly based on the initial dissolution rates to make the theoretical treatment easier. However, with the progress of dissolution the dissolution rate changes with the changes in the surface area and bulk properties of the oxide particles, and also with increasing concentrations of dissolved species in solution. For engineering purposes the extent of dissolution must be

followed from start to completion as a function of time, pH, and ligand concentrations.

In the investigation reported here, copper(II) oxide CuO was chosen as a nonferrous oxide, and CuO powder was formed into a disk specimen by sintering to maintain a constant surface area throughout dissolution. The dissolution of the CuO disk specimen in EDTA solutions resulted in linear dissolved Cu(II) concentration vs. time curves at low pH and parabolic curves at high pH, and the dissolution rates showed a maximum at a specific pH. A model developed for the dissolution of magnetite in EDTA solutions [24-26], where the coupling of metal and oxide ion transfer is considered, appears able to explain and reproduce the observed behaviors [41]. Comprehensive descriptions and full discussion of the results of our investigation will be made here.

2. Materials and methods

2.1. Preparation of copper(II) oxide disk specimen

Commercial copper(II) oxide CuO powder reagent from Kanto Chemical Co., Tokyo, was pressed at 250 kg cm^{-2} into a disk, 16 mm in diameter and 5 mm thick, and heated at 1000°C in the atmosphere for 5 h to sinter. The disk was embedded in resin, and the disk cross-section was exposed by grinding. The exposed surface area *S* of the disk, whose diameter had increased to 16.2 mm by the sintering, was 2.06×10^{-4} m^2.

2.2. Dissolution measurement

The dissolving solutions were mainly 0.475 dm^3 of 3.0×10^{-3} mol dm^{-3} EDTA – 0.1 mol dm^{-3} $NaClO_4$ mixtures. To examine the effect of EDTA concentrations on dissolution, EDTA concentrations lower than 3.0×10^{-3} mol dm^{-3} were employed. The reaction vessel was a 0.5 dm^3 Pyrex container with a Teflon lid with holes for a pH electrode, a temperature sensor, and a reflux condenser that was open to the air, for acid/base supply to adjust pH, and for sampling. The dissolving solution was kept at 80°C with a ribbon heater wound around the container and stirred with a magnetic stirrer. The solution pH was adjusted by adding NaOH or $HClO_4$ solution, and maintained constant with a pH stat. Dissolution experiments were started by dipping the specimen in solution, followed by withdrawing 2 or 5 cm^3 of solution every hour and

measuring the concentration of Cu(II) by atomic absorption spectrometry. The same disk specimen was used repeatedly for different dissolution experiments.

3. Results and discussion

3.1. Dissolution kinetics

Fig. 1 shows the change in the dissolved Cu(II) concentration with time for various pH values. Not all the data, which will appear in Fig. 2, are shown here to make the figure simple. The surface area of the specimen was constant throughout the run as will be discussed below. The highest concentration of Cu(II) dissolved was 1.5×10^{-3} mol dm^{-3} and the concentration of free EDTA can also be regarded as constant throughout the run as more than 90% of the EDTA added (3.0×10^{-3} mol dm^{-3}) remained uncomplexed. The concentration vs. time curves are linear at low pH ($\leq$ 7) and nonlinear at high pH ($\geq$ 8). In the low pH region where the linear kinetics was observed, the concentration of dissolved Cu(II) increases with increasing pH, but in the high pH region where the nonlinear kinetics was observed, the concentration of dissolved Cu(II) decreases with pH.

To show the effect of pH on dissolution, the dissolved Cu(II) concentration after 5 h were plotted against pH in Fig. 2. Results that are not shown in Fig. 1 are also included in Fig. 2. At the same pH the data show some scatter with repeated use of the same specimen, but the scatter is random with respect to the series of experimental runs. The dissolved Cu(II) concentration after 5 h attains a maximum at pH 7-8. At other dissolution times, estimates from Fig. 1 also show the pH peaks: with shorter dissolution times (< 5 h), the peak is less sharp and the peak position shifts to slightly higher pH due to the relatively large dissolution rate at high pH; and with longer dissolution times (> 5 h), the peak becomes sharper due to the decrease in the dissolution rate with time at high pH. Fig. 2 also indicates that without EDTA there is no dissolution at pH 5.5-11 (× mark).

The effect of EDTA concentrations on the dissolution kinetics at pH 5.5 is shown in Fig. 3. High concentrations of EDTA result in high concentrations of dissolved Cu(II), and it is clear that EDTA promotes the dissolution of Cu(II).

3.2. CuO disk surface during dissolution

For this investigation a disk specimen was used to avoid changes in the surface area and dissolution properties during dissolution. Electron microscopy showed that the disk specimen is a sintered product of CuO particles with different sizes and shapes (Fig. 4a). After a dissolution experiment, there was no further development of tunnels or channels due to preferential dissolution of reactive sites (particles) deep in the disk (Fig. 4b). Also repeated dissolution experiments with this same specimen gave similar results. It is likely that the initial surface roughness and hence surface area and the dissolution properties of the disk specimen did not change with the progress of dissolution, indicating "steady-state surface morphologies" [42].

This can be interpreted as follows: the preferential dissolution of reactive sites in the disk creates holes, the dissolving agent EDTA is supplied only with difficulty to these holes, and further dissolution stops here, while the dissolution of less reactive sites in regions accessible to the dissolving solution becomes significant. These microprocesses repeat, and the disk specimen dissolves homogeneously without changing the surface area throughout the EDTA exposure, as the linear kinetics in Fig. 1 indicate (pH 4-7). The nonlinear kinetics in Fig. 1 (pH 8, 8.5, 9, 9.5, 10) were also obtained with the constant surface area.

As a result, changes in the surface area and dissolution properties of the disk specimen need not be considered in the modeling.

3.3. Dissolution model

This investigation aims to develop a model of CuO dissolution for engineering purposes which enables assessment and prediction of the extent of dissolution as a function of a wide range of times, pH, and EDTA concentrations. Here, a model developed by the authors for the dissolution of magnetite in EDTA solutions [24-26] may be applied.

The following pathways (steps) are proposed to describe the dissolution behavior observed in this investigation.

$$\text{-CuO} + \text{H}_n\text{Y}^{(4-n)-} \underset{k_{-1}}{\overset{k_1}{\rightleftharpoons}} \text{CuY}^{2-} + n\text{H}^{+} + \text{-O}^{2-} \quad (1)$$

$$\text{-O}^{2-} + 2\text{H}^{+} \xrightarrow{k_2} \text{H}_2\text{O} \quad (2)$$

In step (1) it is assumed that copper(II) and oxide ion sites on the oxide behave as a –CuO pair. An *n*-protonated EDTA species $H_nY^{(4-n)-}$ transfers a copper(II) ion to the solution by forming an EDTA chelate CuY^{2-} with the liberation of *n* protons and leaves a "lone oxide ion" $–O^{2-}$ on the oxide, this proceeds with the rate constant k_1.

Step (1) may be regarded as differential dissolution of ions from the surface of a sparingly soluble ionic crystal [43]. Smaller cations (Cu^{2+}) have higher affinities for water than larger anions (O^{2-}), and Cu^{2+} ions have a tendency to dissolve preferentially in water, and this tendency is enhanced by the chelate formation with EDTA. The forward reaction in step (1) does not satisfy the electroneutrality condition as the dissolved copper(II) ions provide 2+ excess positive charges to the solution and as the "lone oxide ions" $–O^{2-}$ left behind provide 2- excess negative charges to the solid. Hence, the products in step (1) are unstable, and the amount of $–O^{2-}$ would be very small, not normally detectable in the reacting system.

Here, however, for further dissolution to occur, oxide ions must also dissolve, satisfying electric neutrality, and the successive reaction in step (2) is proposed to achieve this; two protons attach to the "lone oxide ion" to form water with the rate constant k_2. As a result, the transfer of copper(II) and oxide ions from solid to solution is coupled, and the amounts of charges they carry are equal. For step (1) the backward reaction with the rate constant k_{-1} is assumed, which also recovers the electric balance. In the backward reaction, equilibrium of CuY chelates in solution may participate, but such a micromechanism is not expressed in Eq. (1).

In chemical reaction kinetics, it is common that reactants form an intermediate complex [44]. Here the "lone oxide ions" in step (1) are unstable, reactive dissolution intermediates, which exist only temporarily. However, the overall dissolution given as the sum of steps (1) and (2) is "far from equilibrium" as the solubility calculations in the next section indicate, and practically there is no backward reaction for the overall dissolution reaction.

The simple lattice Cu^{2+} and O^{2-} ion sites were considered as the reacting sites in the

dissolution, however, there can be other types of sites on the CuO surface due to (de)protonation of the surface hydroxyl groups and ion adsorption. The surface speciation reactions are rapid compared with the dissolution, and all kinds of surface sites are in equilibrium with the Cu^{2+} and O^{2-} ion sites. The net species transferred from solid to solution by dissolution are Cu^{2+} and O^{2-} ions. These are the reasons why the simple lattice Cu^{2+} and O^{2-} ion sites were chosen as sites for dissolution. If dissolution occurs via other types of sites, which are in acid-base equilibria with the Cu^{2+} and O^{2-} ion sites, the pH dependence of the dissolution is determined also by the protons participating in the formation of those sites. Eq. (1) considers protons released by the deprotonation of EDTA only, but other protons for surface speciation can be added in Eq. (1), if necessary.

As the "lone oxide ions" are unstable, very minor species, their concentration (surface density) may be obtained by applying the principle of stationary states [44] as follows (the electric charges on EDTA species and chelates will be disregarded for simplification):

$$d[\text{-O}^{2-}]/dt = k_1[\text{-CuO}][\text{H}_n\text{Y}] - k_{-1}[\text{CuY}][\text{H}^+]^n[\text{-O}^{2-}] - k_2[\text{-O}^{2-}][\text{H}^+]^2 = 0 \quad (3)$$

$$\therefore [\text{-O}^{2-}] = \frac{k_1[-\text{CuO}][\text{Y}]_\text{T}\,\alpha_{4-n}}{k_{-1}[\text{CuY}][\text{H}^+]^n + k_2[\text{H}^+]^2} \quad (4)$$

Here, $[\text{Y}]_\text{T}$ denotes the total concentration of free EDTA (CuY chelate is excluded), and $\alpha_{4\text{-}n}$ denotes the fraction of H_nY as given by

$$\alpha_{4\text{-}n} = \frac{K_1 \ldots K_{4-n}[\text{H}^+]^n}{K_1K_2K_3K_4 + K_1K_2K_3[\text{H}^+] + K_1K_2[\text{H}^+]^2 + K_1[\text{H}^+]^3 + [\text{H}^+]^4} \quad (5)$$

where K_1-K_4 are the first to fourth deprotonation constants of EDTA and the $K_1 \ldots K_{4-n}$ term is $K_1K_2K_3K_4$ for n = 0, $K_1K_2K_3$ for n = 1, K_1K_2 for n =2, K_1 for n = 3, and 1 for n = 4.

The total concentration of free EDTA $[\text{Y}]_\text{T}$ is actually equal to the total concentration of EDTA added to the system (3.0×10^{-3} mol dm^{-3}), because the amount of

EDTA consumed by the formation of CuY chelate is less than 10% of the added EDTA as described above.

The rate of dissolution of the CuO disk with surface area S and solution volume V is given by

$$(V/S)\mathrm{d[CuY]}/\mathrm{d}t = k_1[\text{-CuO}][\mathrm{Y}]_\mathrm{T}\alpha_{4-n} - k_{-1}[\mathrm{CuY}][\mathrm{H^+}]^n[\mathrm{-O^{2-}}]$$

$$= \frac{k_1 k_2[-\mathrm{CuO}][\mathrm{Y}]_\mathrm{T}\,\alpha_{4-n}[\mathrm{H^+}]^{2-n}}{k_{-1}[\mathrm{CuY}] + k_2[\mathrm{H^+}]^{2-n}} \qquad (6)$$

3.4. Time variations in dissolved Cu(II) concentration

Rate Eq. (6) can be simplified by considering the proton concentration as:

At low pH where $k_{-1}[\mathrm{CuY}] << k_2[\mathrm{H^+}]^{2-n}$ (n may be regarded to be less than 2 as will be explained later),

$$\mathrm{d[CuY]}/\mathrm{d}t = k_1[\text{-CuO}][\mathrm{Y}]_\mathrm{T}\alpha_{4-n}(S/V) \qquad (7)$$

The right-hand side of Eq. (7) is constant at a pH, and this equation is integrated to:

$$[\mathrm{CuY}] = k_1[\text{-CuO}][\mathrm{Y}]_\mathrm{T}\alpha_{4-n}(S/V)t = k't \qquad (8)$$

Here k' [$=k_1[\text{-CuO}][\mathrm{Y}]_\mathrm{T}\alpha_{4-n}(S/V)$] is the composite rate constant. Eq. (8) explains the linear kinetics at pH ≤ 7 in Fig. 1, as the dissolved Cu(II) is the CuY chelate ([Cu(II)] = [CuY]). The values of k' are obtained from the slope of the linear [Cu(II)] vs. time relations in Fig. 1.

At high pH where $k_{-1}[\mathrm{CuY}] >> k_2[\mathrm{H^+}]^{2-n}$,

$$\mathrm{d[CuY]}/\mathrm{d}t = k_1k_2[\text{-CuO}][\mathrm{Y}]_\mathrm{T}[\mathrm{H^+}]^{2-n}\alpha_{4-n}(S/V)(k_{-1}[\mathrm{CuY}]) \qquad (9)$$

Integration of Eq. (9) leads to:

$$[\mathrm{CuY}]^2 = 2\,k_1k_2[\text{-CuO}][\mathrm{Y}]_\mathrm{T}[\mathrm{H^+}]^{2-n}\alpha_{4-n}S/(Vk_{-1})\mathrm{t} = 2k''t \qquad (10)$$

Here k" [$=k_1k_2$[-CuO][Y]$_T$[H^+]$^{2-n}\alpha_{4-n}S/(Vk_{-1})$] is the composite rate constant, and Eq. (10) expresses parabolic kinetics. The data which showed nonlinear kinetics in Fig. 1 at pH $\geq$ 8.5 obey the parabolic rate law Eq. (10). The values of k" are determined from the slope of the linear [Cu(II)]^2 vs. time relations in Fig. 5.

The data at pH 7.5 and 8.0 were not used because they are in a transition region and did not conform to either the linear or parabolic relations.

The model here considers that at high pH the rate of the reaction in step (2) is negligible compared with that of the backward reaction in step (1), but it is not negligible with the net reaction rate in step (1) (forward reaction rate minus backward reaction rate). Rather the reaction in step (2) is fast because the unstable reactive intermediate "lone oxide ions" $-O^{2-}$ react, and the net $-O^{2-}$ formed by the reactions in step (1) thus instantly disappear by the reaction in step (2). This is the reason why the parabolic rate law was obtained.

Parabolic dissolution has also been described for silicates [2-4,14,15] and ascribed to a growing surface layer. The surface layer was suggested to be partially altered primary mineral or a layer of product precipitated from solution. If the diffusion of solutes through this surface layer is rate controlling, increasing layer thickness would result in a deceleration of dissolution. This growing surface-layer mechanism was also applied to the parabolic kinetics of proton-promoted dissolution of hydrous iron(III) oxide [45]. However, the dissolved Cu(II) ions cannot have precipitated as hydroxides or in other forms in the presence of 3.0×10^{-3} mol dm^{-3} EDTA because the solubility calculations with the solubility product K_s of Cu(OH)$_2$ (1.5×10^{-20} mol^3 dm^{-9}), the stability constants K_c of CuY (6.3×10^{18} mol^{-1} dm^3), and the deprotonation constants K_1-K_4 of EDTA (values will be shown in the next section) indicate that they are completely complexed with EDTA and masked from precipitation in the whole pH range examined here. Simple oxides like CuO would not transform into different types of solids during dissolution as the ions which sustain the solid structure transfer to solution by dissolution, different from silicates and aluminosilicates. Actually, the repeated use of the same specimen in this investigation gave similar results, and in another investigation the XPS surface analysis showed that the postulated surface layers did not exist even for aluminosilicates [46].

Another explanation for the parabolic behavior of dissolution considered silicate

samples to be mixtures of ultrafine and large particles [46]. Here, it was proposed that ultrafine particles with large specific surface areas dissolve preferentially due to large excess surface free energies, and after the completion of this dissolution, the transition of dissolution from fast to slow would result in a kind of parabolic behavior. However, in this investigation it was shown that the surface area of the disk specimen remains constant throughout dissolution; sintered large and small particles in the disk do not dissolve independently, preserving "steady-state surface morphologies".

Other investigations [47,48] have considered increasing "backward reaction" rates due to increasing concentrations of dissolved species in solution to explain the deceleratory, parabolic dissolution. Recently it was reported that the dissolution rate of aluminosilicates is reduced by increasing dissolved aluminum concentrations [49,50]. In those investigations, however, the back reaction with respect to the overall reaction was proposed, which becomes significant only near equilibrium conditions, different from the mechanism proposed in this paper. One investigation showed deceleratory kinetics even with little dissolution products in continuous-flow systems where dissolution products were removed continuously [51].

In many dissolution modeling studies, the initial dissolution rates have been used because of the ease of theoretical treatment, as actually the rate of dissolution is affected by the changes in the surface area. Here, the sintered CuO disk specimen of which surface area does not change during dissolution was used to establish the time course of the dissolved Cu(II) concentration and the initial rates alone were not modeled.

3.5. Effect of pH

The values of k' obtained from the slope of the linear [Cu(II)] vs. time relations (pH 4-7 curves in Fig. 1) are plotted against pH in Fig. 6. The log k' vs. pH plot is linear and gives the following expression for the composite rate constant k' at pH 4-7:

$$k' = 10^{-5.6}[H^+]^{-0.15} \quad (11)$$

The proton concentration term here corresponds to the theoretical α_{4-n} term in Eq. (8). The fractions of EDTA species α_0-α_4 were calculated from Eq. (5) with the following EDTA deprotonation constants which were obtained by extrapolation to 80°C [24]: K_1 =

$10^{-1.63}$ mol dm^{-3}, $K_2 = 10^{-2.50}$ mol dm^{-3}, $K_3 = 10^{-5.64}$ mol dm^{-3}, $K_4 = 10^{-9.39}$ mol dm^{-3}. The results are shown as function of pH in Fig. 7, and α_3 and α_4 increase with pH from 4 to 7 where *k*' also increases with pH. However, the increases in α_3 and α_4 with pH are far larger than that of *k*' as given by Eq. (11) (Fig. 6), and neither α_3 and α_4 alone explains *k*'. As a result there is no integer *n* value which expresses the theoretical *k*' in Eq. (8).

Fig. 7 shows that α_2 does not change or slightly decreases with pH in the pH region 4-7, and the observed pH dependence of *k*' can be interpreted to be due to the combined contributions of α_2 and α_3. The situation may be that H_2Y and HY attach to the surface simultaneously to dissolve CuO, and the sum of the contributions of α_2 and α_3 would then explain the observed small pH dependence. Hence, *n* is the average number of protons released from the two dissolving EDTA species per EDTA molecule and the value would be between 1 and 2.

The values of *k*" obtained from the slope of the $[Cu(II)]^2$ vs. time relations (Fig. 5) are also plotted against pH in Fig. 6. The linear log *k*" vs. pH plot result in the following expression for the composite rate constant *k*" at pH 8.5-10:

$$k" = 10^{-1.6}[H^+]^{0.85} \qquad (12)$$

This proton concentration term corresponds to the theoretical $[H^+]^{2-n}\alpha_{4-n}$ term in Eq. (10), which is $K_1 \ldots K_{4-n}[H^+]^2/(K_1K_2K_3K_4 + K_1K_2K_3[H+] + K_1K_2[H+]^2 + K_1[H+]^3 + [H+]^4)$. This depends on the proton concentration to the first power in 8.5-10 pH range, agreeing with a decrease in *k*" with pH. The theoretical proton concentration depencence (1.0) however is slightly larger than the observed exponent (0.85) in Eq. (12) (Fig. 6).

Rate Eq. (6) for the entire pH range can be rewritten with *k*' and *k*" as

$$d[CuY]/dt = k'k"/(k'[CuY] + k") \qquad (13)$$

This is integrated to:

$$k'[CuY]^2/2 + k"[CuY] = k'k"t \qquad (14)$$

The theoretical *k*' and *k*" from Eqs. (8) and (10) cannot be applied to Eq, (14),

because the α_{4-n} term which was suggested to be a composite of α_2 and α_3 has not been formulated here. However, the observed *k*' and *k*" in Eqs. (11) and (12) (Fig. 6) are constant at one pH and EDTA concentration with respect to time, and were introduced into Eq. (14) with the assumption that these relations can be extended outside the pH ranges where they were established. Then the dissolved Cu(II) concentration [CuY] at *t* = 5 h was calculated from Eq. (14) as a function of pH. The results are shown as the curve in Fig. 2, which reproduces the peaking dissolution with respect to pH. The pH peak corresponds to the boundary of the pH regions for the linear and parabolic rate equations obtained by simplifying rate Eq. (6).

In most dissolution models, acceleration of dissolution by ligands has been explained in terms of intermediate ligand-surface complexes [52], as described in the introduction. One model considers that the dissolution peak pH is given by (pK_1 + pK_{s1})/2, where K_1 and K_{s1} are the first deprotonation constants of ligands and surface hydroxyl sites $–OH_2^+$ [27,30,31]. The deprotonation constant K_{s1} of magnetite surface hydroxyl sites was reported to be $10^{-4.4}$ mol dm^{-3} [31]. A similar value, $10^{-4.7}$ mol dm^{-3} at an ionic strength 0.1 mol dm^{-3} ($NaNO_3$) and 25°C, can also be determined by converting the anion exchange equilibrium constant $K_b°$ of base surface hydroxyl groups –OH(b) on magnetite in Tamura et al. [53]. The first deprotonation constant of EDTA (H_4Y) K_1 at 80°C is $10^{-1.63}$ mol dm^{-3} as described above, and the dissolution peak pH is calculated (equation above) to be 3.0-3.2 for magnetite. Borghi et al. [23] obtained a measured value of 3.1 for the peak pH, which coincides with this calculated value. However, other investigations reported a value of 2.3 [22,24-26]. The reason for the different peak pH values is not clear, but the difference between the calculations and the measurements by others [22,24-26] is large.

An analysis of the dissolution mechanism with ligand-surface complexes as intermediates is not simple, and it has been stated that it is not clear whether stable ligand-surface complexes which can be evaluated by measuring the amount of ligand adsorption on oxides are intermediates in the dissolution process or final products that must return to a more reactive uncomplexed state prior to further dissolution [29].

In this investigation the surface complexation approach common in other models was not adopted and formulas for surface complexes as intermediates were not specifically considered in this modeling. However, the relevant rate equation was obtained by assigning appropriate reactants and by considering the "lone oxide ion sites"

as intermediates.

3.6. Effect of EDTA concentration

The *k*' values at pH 5.5 obtained from Fig. 3 are plotted against the EDTA concentration in Fig. 8. The plot is linear, agreeing with the theoretical relation between *k*' and the EDTA concentration $[Y]_T$ from Eq. (8). The α_{4-n} term here however is a composite of α_2 and α_3 as suggested above, and it would also be constant at a pH.

At a constant pH and EDTA concentration, the rate constants *k*' and *k*" are constant with respect to time, and the model rate equations here are appropriate and adequate to reproduce the kinetic data, as the linear and parabolic kinetics could be explained quantitatively.

4. Concluding remarks

The sintered CuO disk specimen was dissolved in EDTA solutions, and surface area of the specimen was constant throughout dissolution, indicating a steady-state surface morphology. As a result, the time change in the concentration of Cu(II) dissolved provided the instantaneous dissolution rate at any point. It was found that the dissolution reaction obeys the linear rate law at pH $\leq$ 7 and the parabolic rate law at pH $\geq$ 8.5. The dissolution rate increased with pH in the linear kinetics region, while it decreased with pH in the parabolic kinetics region, resulting in a pH peak.

In modeling the observed results, it was considered that the copper and oxide ion transfer processes are affected differently by solution conditions (pH and EDTA concentration), and as a result nonstoichiometric lone oxide ion sites are formed. However, the surface nonstoichiometry is maintained stationary, as the principle of stationary states was applied to this nonstoichiometric surface species. The copper and oxide ion transfer processes are then coupled to satisfy the electric neutrality condition, and the dissolution rate is determined by the slower process, i.e., the metal ion transfer with EDTA at low pH and the oxide ion transfer with protons at high pH.

External electric potentials were not applied to the dissolving sintered CiO specimen, but the model proposed here may be compared with electrochemical theories of metal oxide dissolution [1,54-57]. In these theories the metal and oxide ion transfers are

regarded as anode and cathode processes. The anode and cathode processes are affected differently by the applied potential, and the surface composition deviates from the stoichiometric composition. However, the surface nonstoichiometry is maintained, stationary, as the two processes proceed at a rate limited by the slower process. Hence, the anode and cathode processes are coupled and the electric neutrality condition is satisfied.

The effect of electric potentials on the dissolution rate is not considered in this investigation, but the preservation of electric neutrality during dissolution is a key element consideration in the derivation of the model rate equations.

The existence and properties of the lone oxide ion sites is a further issue. Such sites may be difficult to confirm experimentally because their concentration would be very small due to the electric neutrality condition. The assumption of the lone oxide ion sites, however, realizes the very important condition that the dissolution of metal oxides is a transfer of lattice metal ions as well as lattice oxide ions into solution and that the amounts of transferred metal ions and oxide ions much be equal in the charges they carry. The quantitative explanation of the linear and parabolic kinetics of dissolution of CuO and the dissolution rate peak pH was possible by assuming lone oxide ion sites.

Acknowledgements

H.T. expresses thanks to the Rust Science Research Group, Japan, for financial support.

References

[1] J.W. Diggle, Dissolution of oxide phases, in: A.J. Bard (Ed.), Oxides and Oxide Films, vol. 2, Marcel Dekker, New York, 1973, pp. 281-386.

[2] A.F. White, H.C. Classen, Dissolution kinetics of silicate rocks –application to solute modeling, in: E.A. Jenne (Ed.), Chemical Modeling in Aqueous Systems, ACS Symposium Ser. 93, American Chemical Society, Washington, DC, 1979, pp. 447-473.

[3] M.A. Velbel, Influence of surface area, surface characteristics, and solution

composition on feldspar weathering rates, in: J.A. Davis, K.F. Hayes (Eds.), Geochemical Processes at Mineral Surfaces, ACS Symposium Ser. 323, American Chemical Society, Washington, DC, 1986, pp. 615-634.
[4] W. Stumm, G. Furrer, The dissolution of oxides and aluminum silicates; examples of surface-coordination-controlled kinetics, in: W. Stumm (Ed.), Aquatic Surface Chemistry, Wiley, New York, 1987, pp. 197-219.
[5] A.T. Stone, J.J. Morgan, Reductive dissolution of metal oxides, in: W. Stumm (Ed.), Aquatic Surface Chemistry, Wiley, New York, 1987, pp. 221-254.
[6] J. Schott, Modeling of the dissolution of strained and unstrained multiple oxides; the surface speciation approach, in: W. Stumm (Ed.), Aquatic Chemical Kinetics, Wiley, New York, 1990, pp. 337-365.
[7] W. Stumm, E. Wieland, Dissolution of oxide and silicate minerals: rates depend on surface speciation, in: W. Stumm (Ed.), Aquatic Chemical Kinetics, Wiley, New York, 1990, pp. 367-400.
[8] W.H. Casey, B. Bunker, Leaching of mineral and glass surfaces during dissolution, in: M.F. Hochella Jr., A.F. White (Eds.), Mineral-Water Interface Geochemistry, Reviews in Mineralogy, vol. 23, Mineralogical Society of America, Washington, DC, 1990, pp. 397-426.
[9] J.G. Hering, W. Stumm, Oxidative and reductive dissolution of minerals, in: M.F. Hochella Jr., A.F. White (Eds.), Mineral-Water Interface Geochemistry, Reviews in Mineralogy, vol. 23, Mineralogical Society of America, Washington, DC, 1990, pp. 427-465.
[10] W. Stumm, Chemistry of the Solid-Water Interface, Wiley, New York, 1992, p. 157.
[11] F.F. Morel, J.G. Hering, Principles and Applications of Aquatic Chemistry, Wiley, New York, 1993, p. 297.
[12] M.A. Blesa, P.J. Morando, A.E. Regazzoni, Chemical Dissolution of Metal Oxides, CRC Press, Boca Raton, FL, 1994.
[13] W. Stumm, J.J. Morgan, Aquatic Chemistry, third ed., Wiley, New York, 1990, p. 760.
[14] R.M. Cornell, U. Schwertmann, The Iron Oxides, VCH, Weinheim, New York, 1996, p. 267.
[15] J.J. Drever, The Geochemistry of Natural Waters, Prentice-Hall, Upper Saddle River, NJ, 1997, p. 215.

[16] A. Amirbahman, L. Sigg, U. von Gunten, J. Colloid Interf. Sci. 194 (1997) 194.
[17] J.S. LaKind, A.T. Stone, Geochim. Cosmochim. Acta 53 (1989) 961.
[18] R.M. Cornell, P.W. Schindler, Clays Clay Min. 35 (1987) 345.
[19] J. Rubio, E. Matijevi´c, J. Colloid Interf. Sci. 68 (1979) 408.
[20] H,-C, Chang, E. Matijevi´c, J. Colloid Interf. Sci. 92 (1983) 479.
[21] Y. Zhang, N. Kallay, E. Matijevi´c, Langmuir 1 (1985) 201.
[22] I.G. Gorichev, V.S. Dukhanin, N.A. Kipriyanov, Zhurnal Fizicheskoi Khimii 54 (1980) 1341.
[23] E.B. Borghi, A.E. Regazzoni, A.I.J. Maroto, M.A. Blesa, J. Colloid Interf. Sci. 130 (1989) 299.
[24] S. Takasaki, K. Ogura, H. Tamura, M. Nagayama, Zairyo-to-Kankyo (Corros. Engng.) 44 (1995) 86.
[25] S. Takasaki, K. Ogura, H. Tamura, M. Nagayama, Zairyo-to-Kankyo (Corros. Engng.) 45 (1996) 67.
[26] H. Tamura, S. Takasaki, R. Furuichi, Bunseki Kagaku 47 (1998) 397.
[27] E. Baumgartner, M.A. Blesa, A.J.G. Maroto, J. Chem. Soc. Dalton Trans. 1982 (1982) 1649.
[28] M.A. Blesa, H.A. Marinovic, E.C. Baumgartner, A.J.G. Maroto, Inorg. Chem. 26 (1987) 3713.
[29] A.J.G. Maroto, M.A. Blesa, J. Chem. Soc. Faraday Trans. 1 84 (1988) 9.
[30] E.B. Borghi, P.J. Morando, M.A. Blesa, Langmuir 7 (1991) 1652.
[31] E. Baumgartner, J. Romagnolo, M.I. Litter, J. Chem. Soc. Trans. 89 (1993) 1049.
[32] M.A. Blesa, A.J.G. Maroto, P.J. Morando, J. Chem. Soc. Trans. 82 (1986) 2345.
[33] J. Eisenlauer, E. Matijevi´c, J. Colloid Interf. Sci. 75 (1980) 199.
[34] H,-C, Chang, E. Matijevi´c, Finn. Chem. Lett. 1982 (1982) 90.
[35] H,-C, Chang, T.W. Healy, E. Matijevi´c, J. Colloid Interf. Sci. 92 (1983) 469.
[36] M.A. Blesa, E.B. Borghi, A.J.G. Maroto, A.E. Regazzoni, J. Colloid Interf. Sci. 98 (1984) 295.
[37] N. Kallay, E. Matijevi´c, Langmuir 1 (1985) 195.
[38] A.E. Regazzoni, M.A. Blesa, Langmuir 7 (1991) 473.
[39] R. Torres, M.A. Blesa, E. Matijevi´c, J. Colloid Interf. Sci. 131 (1989) 567.
[40] S.M. Kraemer, V.Q. Chiu, J.G. Hering, Environ. Sci. Technol. 32 (1998) 2876.
[41] H. Tamura, N. Ito, S. Takasaki, R. Furuichi, Zairyo-to-Kankyo (Corros. Engng.) 49

(2000) 22.
[42] B. Wehrli, J. Colloid Interf. Sci. 132 (1989) 230.
[43] D.H. Everett, Basic Principles of Colloid Science, The Royal Society of Chemistry, London, 1988, p. 37.
[44] S.R. Logan, Fundamentals of Chemical Kinetics, Longman, Harlow, Essex, 1996, p. 45.
[45] R. Furuichi, N. Sato, G. Okamoto, Chimia 23 (1969) 455.
[46] R.G. Holdren Jr., R.A. Berner, Geochim. Cosmochim. Acta 43 (1979) 1161.
[47] H.C. Helgeson, W.M. Murphy, Math. Geology 15 (1983) 109.
[48] H.C. Helgeson, W.M. Murphy, P. Aagaard, Geochim. Cosmochim. Acta 48 (1984) 2405.
[49] T.E. Burch, K.L. Nagy, A.C. Lasaga, Chem. Geol. 105 (1993) 137.
[50] E.H. Oelkers, J. Schott, J,-L. Devidal, Geochim. Cosmochim. Acta 58 (1994) 2011.
[51] L. Chou, R. Wallast, Geochim. Cosmochim. Acta 48 (1984) 2205.
[52] W. Stumm, Colloids Surfaces 120 (1997) 143.
[53] H. Tamura, N. Katayama, R. Furuichi, Environ. Sci. Technol. 30 (1996) 1198.
[54] H.J. Engell, Z. Physik. Chem. 7 (1956) 158.
[55] D.A. Vermilyea, J. Electrochem. Soc. 113 (1966) 1067.
[56] M. Seo, N. Sato, Boshoku Gijyutsu 24 (1975) 399.
[57] S. Haruyama, K. Masamura, Corros. Sci. 18 (1978) 263.

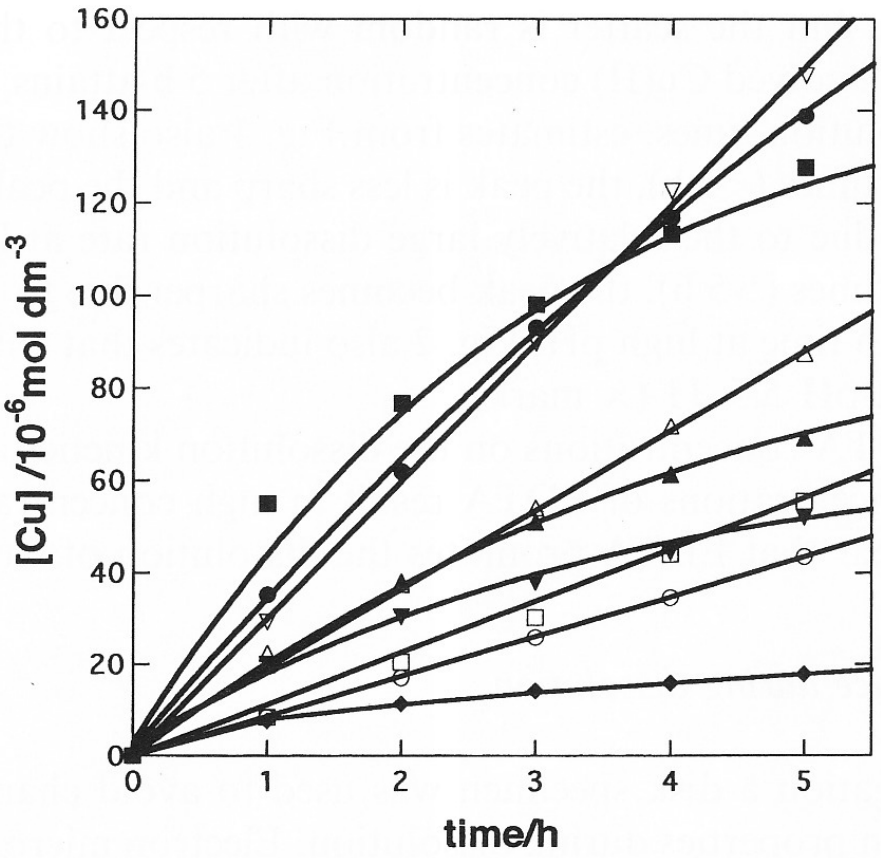

Fig. 1. Time changes in dissolved Cu concentration [Cu(II)] in 3×10^{-3} mol dm^{-3} EDTA solutions at 80°C for different pH: pH = 4 (○), 5 (□), 6 (△), 7 (▽), 8 (●), 8.5 (■), 9 (▲), 9.5 (▼), 10 (◆).

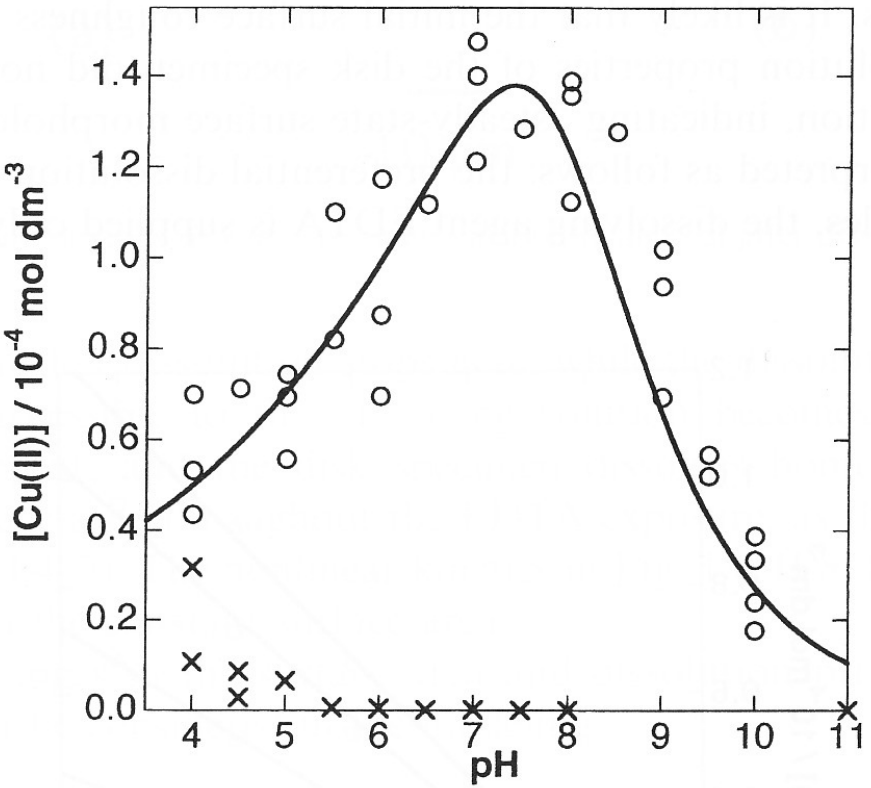

Fig. 2. Relationship between dissolved Cu concentration [Cu(II)] and pH in 3×10^{-3} mol dm^{-3} EDTA solutions at 80°C after 5 h. With EDTA (○), without EDTA (×); curve calculated with Eq. (14).

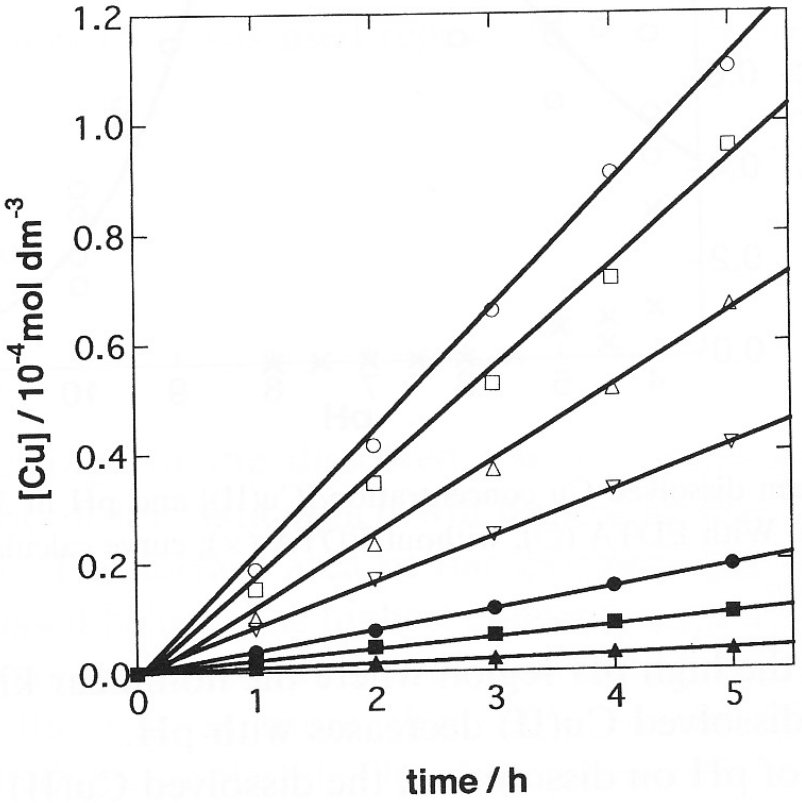

Fig. 3. Time changes in dissolved Cu concentrations [Cu(II)] for different EDTA concentrations [EDTA] at pH 5.5. [EDTA]/10^{-4} mol dm^{-3}: 0.75 (▲), 1.5 (■), 3.0 (●), 6.0 (▽), 10 (△◇), 20 (□), 30 (○).

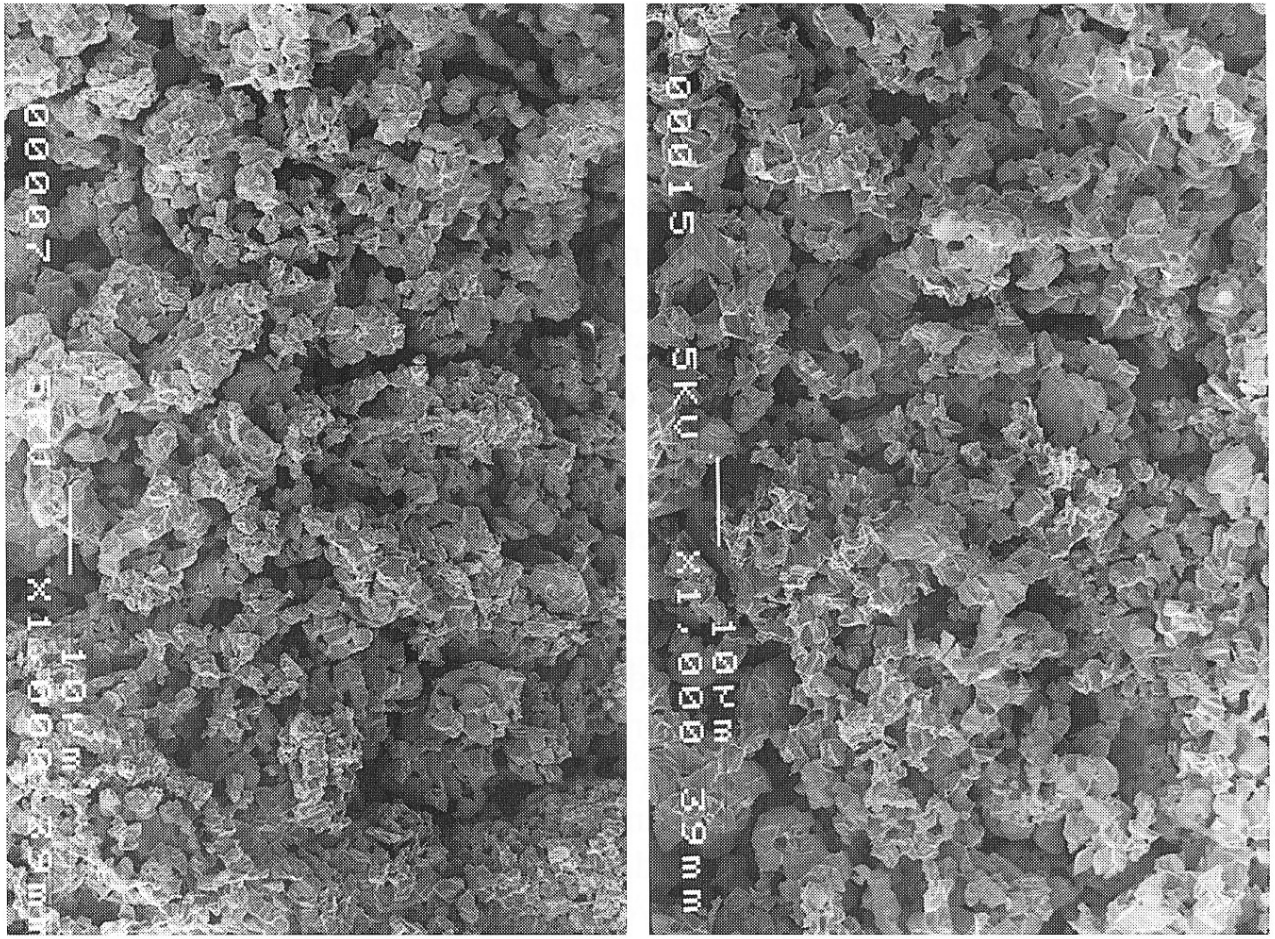

Fig. 4. Electron micrographs of CuO specimen. (a) Before and (b) after dissolution experiment.

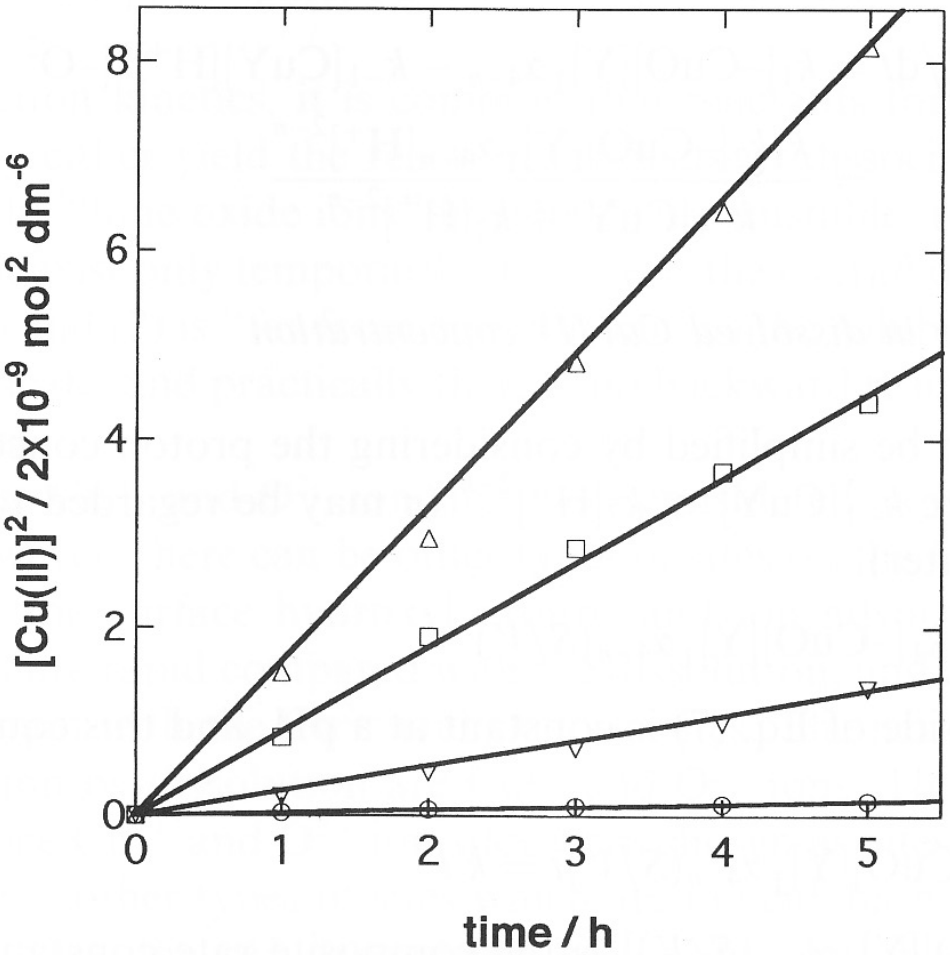

Fig. 5. Plot of $[Cu(II)]^2$ vs. time for different pH: pH = 8.5 (△), 9.0 (□), 9.5 (▽), 10 (○).

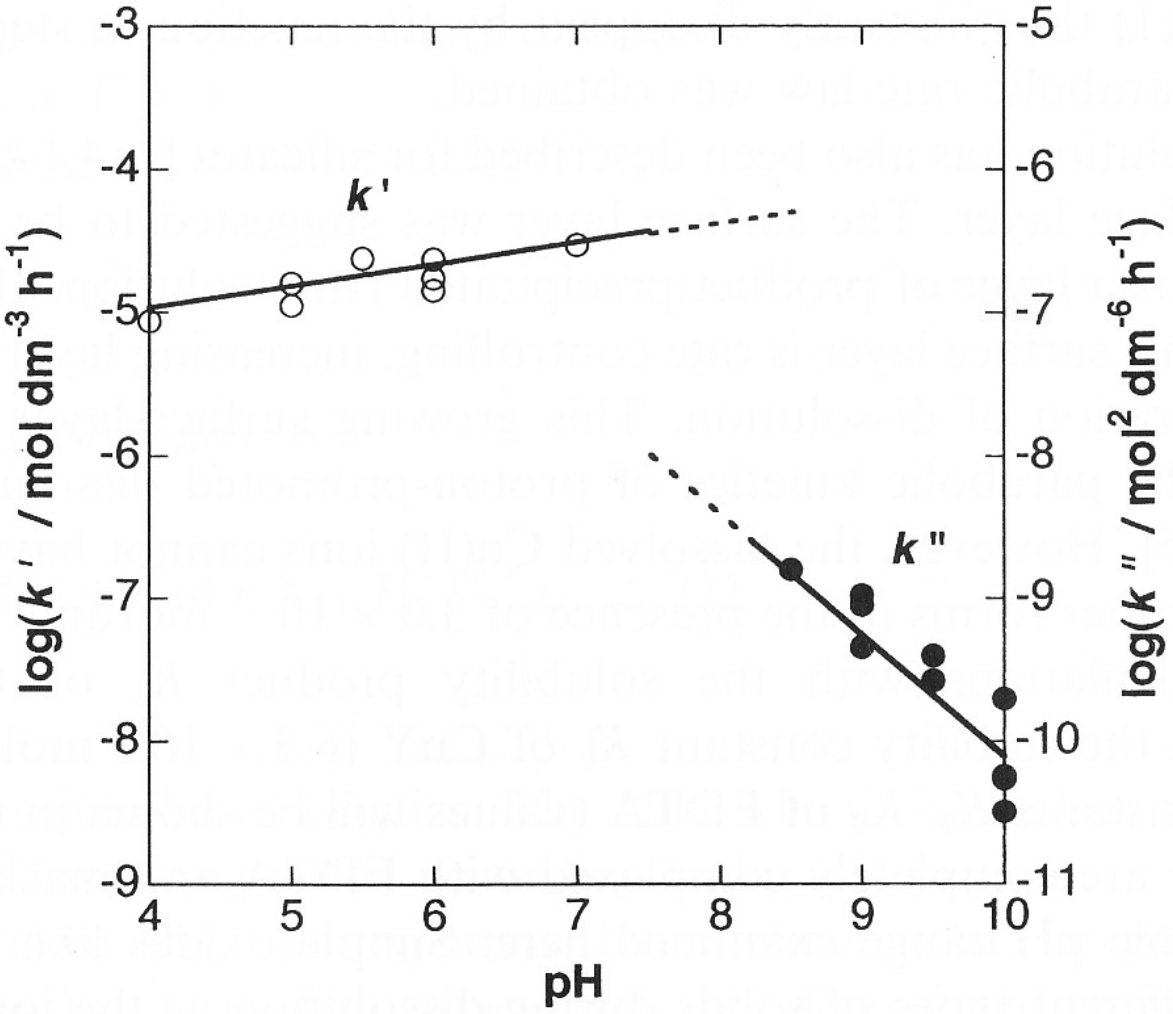

Fig. 6. Relationship between k' or k'' and pH: k' (○) and k'' (●).

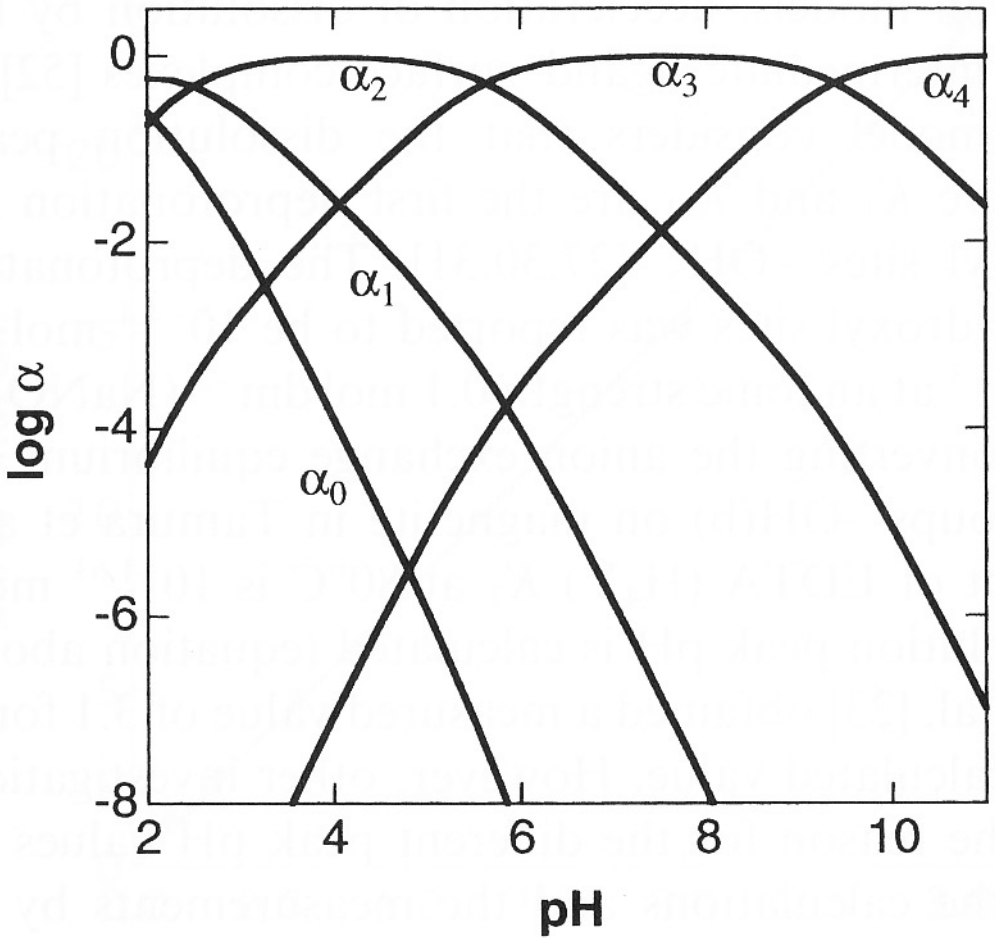

Fig. 7. Plot of the fractions α of EDTA species at 80°C as a function of pH.

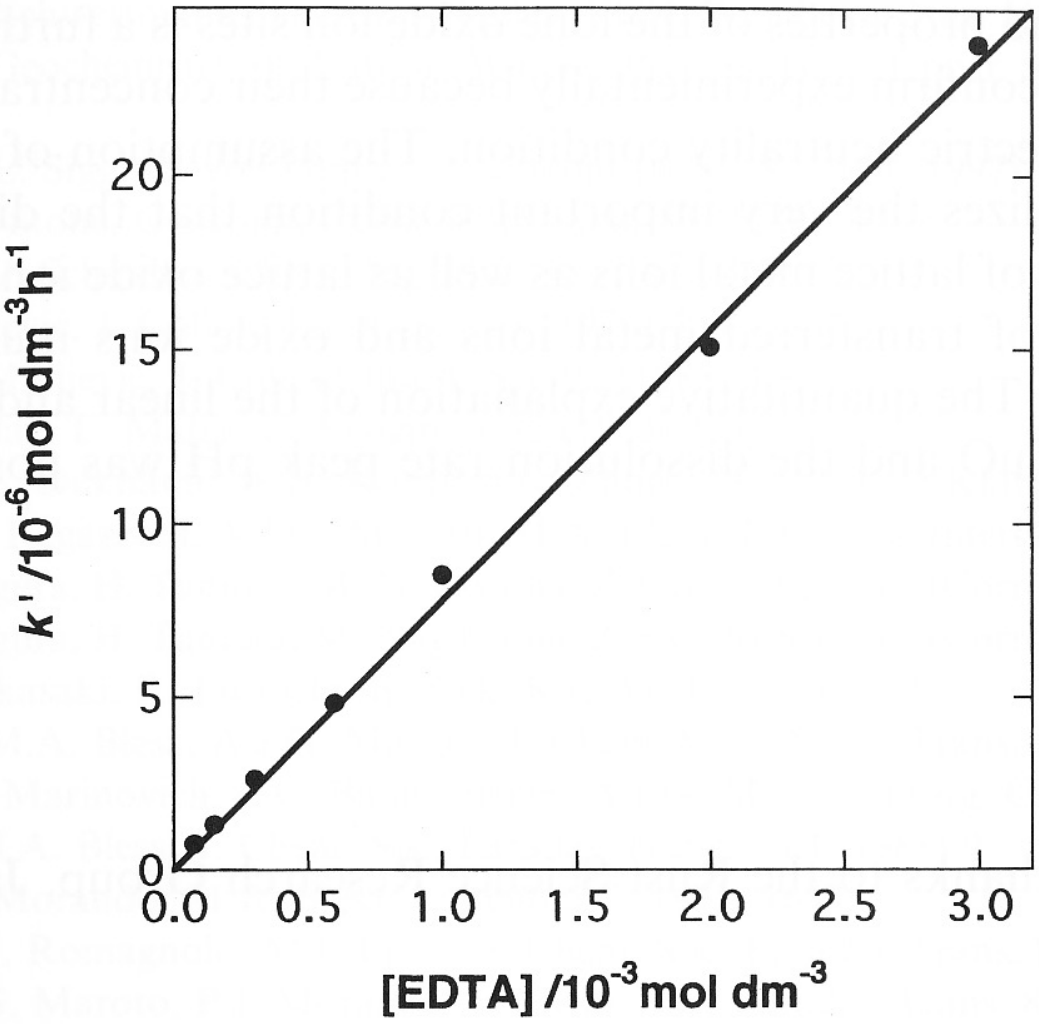

Fig. 8. Relationship between k' and EDTA concentration at pH 5.5.